Sequential Linear Interpolation of Multidimensional Functions

James Z. Chang, *Member, IEEE,* Jan P. Allebach, *Fellow, IEEE,* and Charles A. Bouman, *Member, IEEE*

***Abstract*—We introduce a new approach that we call *sequential linear interpolation* (SLI) for approximating multidimensional nonlinear functions. The SLI is a partially separable grid structure that allows us to allocate more grid points to the regions where the function to be interpolated is more nonlinear. This approach reduces the mean squared error (MSE) between the original and approximated function while retaining much of the computational advantage of the conventional uniform grid interpolation. To obtain the optimal grid point placement for the SLI structure, we appeal to an asymptotic analysis similar to the asymptotic vector quantization (VQ) theory. In the asymptotic analysis, we assume that the number of interpolation grid points is large and the function to be interpolated is smooth. Closed-form expressions for the MSE of the interpolation are obtained from the asymptotic analysis. These expressions are used to guide us in designing the optimal SLI structure. For cases where the assumptions underlying the asymptotic theory are not satisfied, we develop a postprocessing technique to improve the MSE performance of the SLI structure. The SLI technique is applied to the problem of color printer characterization where a highly nonlinear multidimensional function must be efficiently approximated. Our experimental results show that the appropriately designed SLI structure can greatly improve the MSE performance over the conventional uniform grid.**

***Index Terms*— Color transformation, multidimensional interpolation, sequential structure, splines.**

I. Introduction

MANY important problems in image and signal processing require the accurate approximation of nonlinear multidimensional functions. For example, the interpolation of the velocity fields of turbulent fluid flow [1] requires that we approximate nonlinear functions in a multidimensional space. In the areas of computer-aided graphic design and pattern recognition, nonlinear functional approximation techniques [2]–[7] are used to render or represent complicated curves and surfaces. In the problem of color device calibration [8]–[10], we also need to develop efficient schemes to approximate nonlinear color transformations. The objective of this paper is to present a theory of optimal functional approximation and to apply it to the problem of color device characterization and calibration.

Manuscript received June 5, 1995; revised October 16, 1996. This work was supported by Apple Computer, Inc. The associate editor coordinating the review of this manuscript and approving it for publication was Prof. Andrew Yagle.

J. Z. Chang is with Color Savvy Systems Incorporated, Springboro, OH 45066 USA (e-mail: jzchang@ix.netcom.com).

J. P. Allebach and C. A. Bouman are with the School of Electrical and Computer Engineering, Purdue University, West Lafayette, IN 47907-1285 USA.

Publisher Item Identifier S 1057-7149(97)06244-1.

Many authors have studied the problem of efficient approximation of a nonlinear function in the context of finding the optimal positions of the interpolation grid points. In the area of curve fitting with piecewise linear functions, Cantoni [11] presented a method for obtaining the optimal grid points using an iterative random search algorithm. Pavlidis [12], [13] used Newton's method and functional iteration techniques to locate the optimal grid points. These algorithms are further extended by Abdelmalek [14] to improve the computational efficiency. In [2], Hamann and Chen developed a parameter called *curvature measure* and used it to allocate more interpolation grid points to the more nonlinear regions of the curve. Lu and Milios [3], [4] and Sato [5] developed techniques for obtaining the optimal piecewise linear approximation of planar curves in the field of pattern recognition. In the area of higher order spline fitting, Kitson [6] and Qamar [7] presented iterative techniques to reduce the approximation errors in the problem of curve and surface fitting using B-splines and cubic splines, respectively. Carey and Dinh [15] took an equidistribution approach to the one-dimensional (1-D) problem of determining an optimal grid point distribution for use in solving two point boundary value problems via finite differences. Baines [16] developed iterative methods for optimal grid point placement in 1-D and two-dimensional (2-D) for discontinuous piecewise linear approximation of functions. He also cited additional methods based on the equidistribution approach.

In this paper, we present the sequential linear interpolation (SLI) structure for the efficient interpolation of multidimensional nonlinear functions. The approximating functions that we use are multidimensional linear splines with a partially separable structure. As shown in Fig. 1(a), the conventional grid for interpolation is a uniform grid. Intuitively, for linear interpolation we want to place more grid points in regions where the function is more nonlinear and fewer grid points in regions where it is linear. Obviously, with the uniform grid structure, we cannot do this. However, interpolation with a uniform grid structure is very efficient to implement compared to interpolation with unstructured grid points in the 2-D space, which would require a search for neighboring grid points to be used in the computation of each interpolated output value. We propose the alternative SLI grid structure shown in Fig. 1(b). The grid points in this structure are constrained to fall along grid lines that are parallel to the x_2 axis. This structure allows for nonuniform placement of grid points, while retaining much of the computational advantage of conventional bilinear interpolation on a uniform grid. This SLI grid structure can be easily generalized to higher dimensional cases.

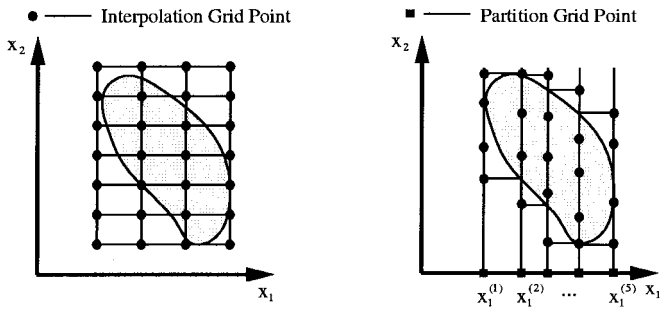

Fig. 1. Grid structures for (a) regular and (b) sequential interpolation.

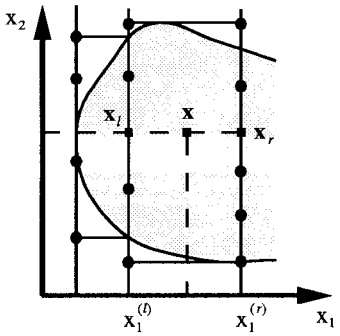

Fig. 2. Sequential linear interpolation (SLI) scheme.

To obtain the optimal SLI grid structure, we appeal to an asymptotic analysis that yields a closed-form relationship between the interpolation error and the number and positions of the grid points. The theory we develop is in many ways analogous to the theory of asymptotic vector quantization (VQ) [17]–[19]. In VQ, an N level K-dimensional (K-D) quantizer is defined as a mapping Q that maps each input vector $\mathbf{x} \in \mathbb{R}^K$ to a reproduction vector $\hat{\mathbf{x}} = Q(\mathbf{x})$ drawn from a set $\mathcal{C}$ of N vectors, which is called a *codebook*. To optimally design a vector quantizer, we need to find the codebook $\mathcal{C}$ and the mapping rule Q so that the expected error between the original and mapped vectors are minimized under a certain distortion measure. In interpolation, we consider that a K-D function $f(\mathbf{x})$ is represented by a set of pairs $(\mathbf{x}, f(\mathbf{x}))$, $\mathbf{x} \in \mathbb{R}^K$, and to design an interpolation grid with N points, we find a set $\mathcal{G}$ of N grid points that minimizes the expected error between the original and interpolated functions under a certain distortion measure and the method of interpolation.

In this paper, we choose linear interpolation since it is efficient to implement; and we choose weighted mean-squared error (MSE) as our distortion measure. Together, these choices allow us to obtain mathematically tractable results. In some applications, a minimax distortion measure may be more appropriate. With such a measure, it is possible to obtain results that are analogous to, but substantially different from, those derived here [20]. Our development closely parallels the theory previously presented for optimal sequential scalar quantization (SSQ) of vectors [21]–[23]. However, our analysis extends these previous results since it accounts for the approximation error of linear splines; and it asymptotically achieves the optimal performance in terms of the error criterion under the constraints of the SLI structure. It is interesting to compare our results with those obtained previously by Carey and Dinh [15]. They used a Fourier series approach to obtain an unweighted H^m-seminorm error estimate in terms of the grid point distribution for 1-D functions with a continuous, piecewise polynomial of degree k. A Euler variational argument is then applied to minimize this error estimate. We use a completely different approach based on Hölder's inequality to find the grid point distribution that minimizes the weighted MSE in continuous, piecewise linear interpolation of a K-D function. With no weighting of the error and $K = 1$, our results match theirs with $m = 0$ and $k = 1$.

The asymptotic design theory gives us closed-form relationships between the number and positions of the grid points and the interpolation error. We can use these relationships to directly design the optimal SLI structure. In Section II, we will see that implementation of the SLI structure in Fig. 1(b) requires the same number of multiplications as the conventional interpolation structure in Fig. 1(a), which is based on a uniform grid. Furthermore, as in the case of the conventional interpolation structure, the SLI structure also guarantees that the approximated function is continuous, which is important in many applications. The advantage of the SLI structure is that it can interpolate the function more accurately given a fixed number of interpolation grid points.

In the next section, we present the SLI structure and its implementation. In Section III, we present the asymptotic design theory. This theory is for scalar-valued multidimensional functions. In [24], we extend the theory to the case of vector-valued functions. In Section IV, we present a postprocessing technique to account for the practical situation where the assumptions for the asymptotic analysis are not well satisfied. The application of the SLI technique to the problem of color printer characterization and calibration is presented in Section V.

II. Sequential Linear Interpolation

In this section, we present the SLI structure and its implementation. We begin with a 2-D SLI structure and then generalize the structure to higher dimensional functions. For simplicity, here we present the SLI structure for scalar-valued functions. In [24], we expand the structure to vector-valued functions. In the vector-valued case, we can either independently design an SLI structure for each component function, or jointly design a single SLI structure for all the component functions.

Let $y = f(\mathbf{x})$ be a 2-D scalar-valued function, where $\mathbf{x} = (x_1, x_2)$ is a vector in $\mathbb{R}^2$. We further assume that the domain of $f(\mathbf{x})$ is bounded. To sequentially allocate grid points to the domain of $f(\mathbf{x})$, we first place n_1 partition grid points, $x_1^{(1)}, x_1^{(2)}, \cdots, x_1^{(n_1)}$, onto the x_1 axis as shown in Fig. 1(b) for $n_1 = 5$. These grid points can be placed nonuniformly according to the characteristics of the function being interpolated. The partition grid points on the x_1 axis correspond to n_1 grid lines in the 2-D domain. As also shown in Fig. 1(b), we further place $N_1(i)$ 1-D interpolation grid points on the ith grid line for $i = 1, 2, \cdots, n_1$, according to

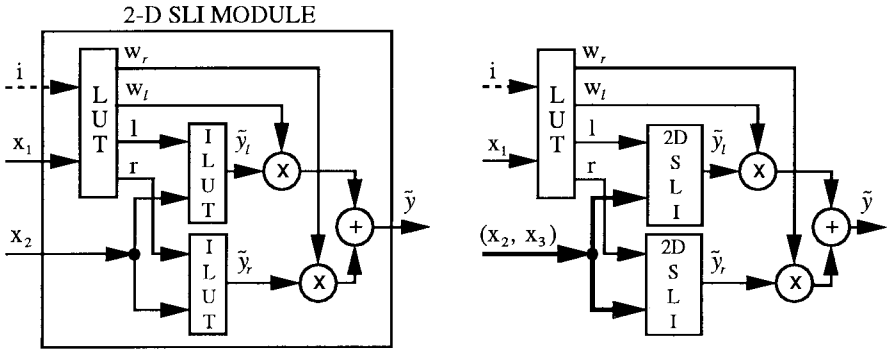

(a) (b)

Fig. 3. LUT implementation of (a) 2-D and (b) 3-D sequential linear interpolation.

the characteristics of the function. We note from the figure that some of the grid points are placed outside the domain of the function to ensure that all the points in the domain are properly interpolated by the SLI implementation. The method for finding the functional values for these grid points will depend on the specific application. Suppose that N_2 is the total number of 2-D interpolation grid points, then the $N_1(i)$'s must satisfy the constraint

$$N_2 = \sum_{i=1}^{n_1} N_1(i). \tag{1}$$

The output y's at these interpolation grid points are stored for piecewise linear interpolation on the grid lines parallel to the x_2 axis.

To find the approximation $\tilde{y} = \tilde{f}(\mathbf{x})$ at an arbitrary point $\mathbf{x} = (x_1, x_2)$, $\mathbf{x}$ is first projected onto the two adjacent grid lines at $x_1^{(l)}$ and $x_1^{(r)}$, respectively, as depicted in Fig. 2. These projection points are $\mathbf{x}_l$ and $\mathbf{x}_r$. Linear interpolations are performed along the grid lines at $x_1^{(l)}$ and $x_1^{(r)}$ to obtain approximate function outputs $\tilde{y}_l$ and $\tilde{y}_r$ at $\mathbf{x}_l$ and $\mathbf{x}_r$, respectively. The values $\tilde{y}_l$ and $\tilde{y}_r$ are then used to linearly interpolate the value $\tilde{y}$ at $\mathbf{x}$. The implementation of the sequential linear interpolation process is depicted in Fig. 3(a). The linear interpolations on the grid lines can be implemented by a pair of interpolative look-up tables (ILUT). The projection step can be implemented by passing the first component x_1 into a LUT to obtain the indices l and r which identify the grid lines at $x_1^{(l)}$ and $x_1^{(r)}$. These indices and x_2 are the inputs to the ILUT's which compute the interpolated values $\tilde{y}_l$ and $\tilde{y}_r$. These outputs are then linearly combined to obtain $\tilde{y}$. That is

$$\tilde{y} = w_l \tilde{y}_l + w_r \tilde{y}_r \tag{2}$$

where the coefficients

$$w_r = \frac{x_1 - x_1^{(l)}}{x_1^{(r)} - x_1^{(l)}} \tag{3}$$

and

$$w_l = 1 - w_r \tag{4}$$

are also obtained from the first LUT. If the 2-D SLI structure is used as a module in a larger structure—e.g., a three-dimensional (3-D) SLI structure—then an optional index input i is also required.

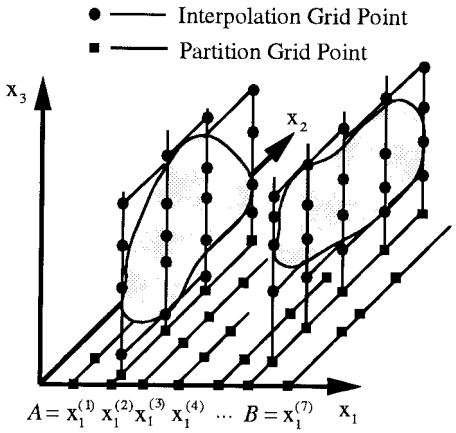

Fig. 4. Illustration of a 3-D SLI grid structure.

The SLI discussed above may be generalized to 3-D functions. For a scalar-valued 3-D function $y = f(\mathbf{x})$, where $\mathbf{x} = (x_1, x_2, x_3)$ is in a bounded domain in $\mathbb{R}^3$, we first place n_1 partition grid points onto the x_1 axis. These grid points will generate n_1 grid planes in the x_2-x_3 space. On each of these grid planes, we construct a 2-D SLI structure as previously described. This process is illustrated in Fig. 4 for $n_1 = 7$ with two of the seven 2-D SLI grid planes shown. To obtain the output value for a certain point $\mathbf{x}$, we first project it onto the two adjacent grid planes. The projection process is implemented by a LUT, as depicted in Fig. 3(b). The function values at the projected points on those grid planes can be obtained by the 2-D SLI modules implemented on those grid planes. These values are then linearly combined to obtain the desired output using the weights generated by the first LUT. An optional index input i is also shown for use in a higher dimensional SLI structure. From the discussion here, we see that this method can be readily generalized to higher dimensional functions.

III. Asymptotic Design Theory

In this section, we present the asymptotic theory for obtaining the optimal placement of the grid points for the SLI structure to minimize the error between the original and the interpolated function. The error criterion is a special form of MSE developed for the SLI structure. We begin with an

introduction to the asymptotic analysis, and present the error criterion that we want to minimize. Then we present a detailed asymptotic analysis for 1-D SLI, and generalize it to the multidimensional case.

A. Asymptotic Analysis

From the discussion in the last section, we see that to design a 1-D SLI, we only need to obtain the optimal placement of the grid points. For a 2-D SLI, we first need to obtain the number and positions of the partition grid points to be placed on the first axis. Then we need to allocate the number of grid points to each grid line parallel to the second axis which corresponds to a partition grid point on the first axis. After this allocation, the optimal placement of grid points on a grid line parallel to the second axis is itself a 1-D SLI design problem. In general, to design a K-D (K-dimensional) SLI, we need to find the number and positions of the partition grid points to be placed on the first axis. Then we need to allocate the number of interpolation grid points to each $(K-1)$-D SLI that corresponds to a partition grid point on the first axis. Finally, we must optimally design each of these $(K-1)$-D SLI structures. We should note that the performance of the SLI structure does depend on the order in which the axes are partitioned. For simplicity, in this paper, we assume that the axes are partitioned in increasing order, from x_1 to x_K. In practice, it may be necessary to evaluate the performance of SLI structures designed by partitioning the axes in all possible orderings, and then picking the best one, as was done in [21] and [22] for SSQ. The asymptotic theory can be used to estimate the error that results with a particular ordering.

In general, the minimization of MSE for the SLI structure is a nonlinear iterative problem, which cannot be written in closed form in terms of the design parameters and placement of grid points. However, if the number of grid points is allowed to become asymptotically large, then we can extend the asymptotic theory in [17]–[19] to obtain an approximate closed-form solution. The idea behind the asymptotic theory is that the number of grid points is assumed to be large enough so that the function to be interpolated is smooth within each linear interpolation interval. Then the MSE's within each interpolation interval can be obtained in closed form and appropriately summed to yield an approximation to the overall MSE. The asymptotic analysis not only provides intuition about the behavior of the SLI, but also can serve as a valuable guide in the design of the SLI grid structures even if the number of grid points is small.

In the remainder of this section, we assume that the function is scalar valued. The asymptotic analysis for vector-valued functions is presented in [24]. In the next subsection, we present the error criterion used for designing the SLI structure. Then we present the asymptotic analysis to minimize this error criterion.

B. Error Criterion for SLI Design

Suppose that the scalar-valued multidimensional function $f(\mathbf{x})$ is approximated by the SLI implementation $\tilde{f}(\mathbf{x})$. Now we define the error function as

$$\Delta f(\mathbf{x}) = f(\mathbf{x}) - \tilde{f}(\mathbf{x}) \tag{5}$$

and the weighted MSE as

$$\mathcal{E} = \int_{\Omega} W(\mathbf{x}) \|\Delta f(\mathbf{x})\|^2 \, d\mathbf{x} \tag{6}$$

where Ω is the domain of $f(\mathbf{x})$ and $W(\mathbf{x})$ is a nonnegative weighting function. If a straightforward MSE is desired, we can set the weighting function $W(\mathbf{x})$ to one. In general, the choice of $W(\mathbf{x})$ depends on the application. For some applications, we may want to let $W(\mathbf{x})$ be the probability density function of $\mathbf{x}$ so that $\mathcal{E}$ is the true MSE in a probabilistic sense.

Now we consider the 2-D case. From (2) in Section II, we observe that the approximated 2-D function $\tilde{y} = \tilde{f}(\mathbf{x})$ is obtained by linearly combining $\tilde{y}_l$ and $\tilde{y}_r$. As shown in Figs. 2 and 3(a), $\tilde{y}_l$ and $\tilde{y}_r$ are approximations to $f(\mathbf{x}_l)$ and $f(\mathbf{x}_r)$, respectively; and they are obtained by 1-D piecewise linear interpolation along the x_2 coordinate.

Our objective is to decompose the overall error $\Delta f(\mathbf{x})$ into two parts corresponding to the errors introduced by the interpolation along the x_1 and x_2 coordinates, respectively. To accomplish this, we need to resort to the conditions for asymptotic analysis, which assume that the distribution of the grid lines and grid points is dense enough and $f(\mathbf{x})$ is smooth in the sense that all of its second partial derivatives are continuous so that the errors from the 1-D linear interpolation on adjacent grid lines are approximately the same. With this assumption, we define the 1-D interpolation error along the x_2 coordinate of $\mathbf{x}$ by

$$\Delta f_2(\mathbf{x}) \approx f(\mathbf{x}_l) - \tilde{y}_l \approx f(\mathbf{x}_r) - \tilde{y}_r. \tag{7}$$

Then $\tilde{f}(\mathbf{x})$ can be written as

$$\tilde{f}(\mathbf{x}) = w_l f(\mathbf{x}_l) + w_r f(\mathbf{x}_r) - \Delta f_2(\mathbf{x}). \tag{8}$$

We further define the error resulting from interpolation along the x_1 coordinate as

$$\Delta f_1(\mathbf{x}) = f(\mathbf{x}) - [w_l f(\mathbf{x}_l) + w_r f(\mathbf{x}_r)]. \tag{9}$$

Thus, we have

$$\tilde{f}(\mathbf{x}) = f(\mathbf{x}) - [\Delta f_1(\mathbf{x}) + \Delta f_2(\mathbf{x})] \tag{10}$$

and the total error $\Delta f(\mathbf{x})$ is decomposed into

$$\Delta f(\mathbf{x}) = \Delta f_1(\mathbf{x}) + \Delta f_2(\mathbf{x}). \tag{11}$$

With this decomposition, the weighted MSE in (6) may be upper bounded as

$$\begin{aligned} \mathcal{E} &= \int_{\Omega} W(\mathbf{x})[\Delta f_1(\mathbf{x}) + \Delta f_2(\mathbf{x})]^2 \, d\mathbf{x} \\ &= \sum_{i=1}^{2} \int_{\Omega} W(\mathbf{x})[\Delta f_i(\mathbf{x})]^2 \, d\mathbf{x} \\ &\quad + 2 \int_{\Omega} W(\mathbf{x}) \Delta f_1(\mathbf{x}) \Delta f_2(\mathbf{x}) \, d\mathbf{x} \qquad (12) \\ &\leq 2 \sum_{i=1}^{2} \int_{\Omega} W(\mathbf{x})[\Delta f_i(\mathbf{x})]^2 \, d\mathbf{x}. \qquad (13) \end{aligned}$$

Since the integrand of the cross-multiplication error term

of (12) may be negative, it is very difficult to minimize. Therefore, we choose to minimize the error criterion

$$\mathcal{D}_2 = \sum_{i=1}^{2} \int_{\Omega} W(\mathbf{x})[\Delta f_i(\mathbf{x})]^2 \, d\mathbf{x} \tag{14}$$

since it upper bounds $\mathcal{E}/2$. This choice is further justified by the fact that if the interpolation errors $\Delta f_1(\mathbf{x})$ and $\Delta f_2(\mathbf{x})$ are assumed to be independent random variables, then the expected value of their product will be zero. Then neglecting the approximation made in (7), the MSE will be exactly $\mathcal{D}_2$. From our experimental results in Section V, we shall see that we can significantly reduce the MSE due to the interpolation by minimizing $\mathcal{D}_2$.

Generalizing the discussion above to K-D SLI designs, we minimize

$$\mathcal{D}_K = \sum_{i=1}^{K} D_i \tag{15}$$

where

$$D_i = \int_{\Omega} W(\mathbf{x})[\Delta f_i(\mathbf{x})]^2 \, d\mathbf{x} \tag{16}$$

for $i = 1, 2, \cdots, K$. Here, $\Delta f_i(\mathbf{x})$ denotes the error resulting from the linear interpolation along the x_i axis assuming that the values used for interpolation are accurate. In some applications, it may be desirable to modify (15) by adding a weighting factor to each of the K dimensions.

In the following subsections, we present the asymptotic analysis to minimize the error criterion in (15), and thereby obtain the optimal SLI design parameters and functions. We will start with a 1-D asymptotic analysis, and then develop the K-D asymptotic analysis.

C. 1-D SLI Design

In the 1-D asymptotic analysis, the placement of the grid points on a certain grid line is specified by the 1-D interpolation interval density function. Assume that n_1 grid points are allocated to the finite interval $[A, B]$ on the x axis. Let $n_I(x)\,dx$ be the number of interpolation intervals that lie in the interval $[x, x+dx]$. Since n_1 grid points divide the interval $[A, B]$ into $n_1 - 1$ interpolation intervals with grid points at both ends of the interval, we define the 1-D interpolation interval density function on the x axis for $x \in [A, B]$ as

$$\lambda_1(x) = \lim_{n_1 \to \infty} \frac{n_I(x)}{n_1 - 1}. \tag{17}$$

Thus, for sufficiently large n_1, the quantity $(n_1 - 1)\lambda_1(x)\,dx$ is approximately the number of interpolation intervals in $[x, x + dx]$. Therefore, we have

$$\int_A^B \lambda_1(x)\,dx = 1. \tag{18}$$

The objective of 1-D SLI design is to find the optimal $\lambda_1(x)$. The derivation which follows will form the basis for the derivation of the general K-D results presented in the Appendix.

For a 1-D function $f(x)$ defined on the finite interval $[A, B]$, suppose that n_1 grid points x_i, $1 \le i \le n_1$, are placed on the x axis such that $A = x_1 < x_2 < \cdots < x_{n_1} = B$. By applying a result from numerical analysis [25], the interpolation error $\Delta f(x)$ in each interval $[x_i, x_{i+1}]$, for $i = 1, 2, \cdots, n_1 - 1$, can be expressed as

$$\Delta f(x) = (x - x_i)(x - x_{i+1}) \frac{f''(\xi_i)}{2} \tag{19}$$

where $\xi_i \in [x_i, x_{i+1}]$ and in general depends on x. Then the error criterion in (15) for $K = 1$ can be written as

$$\mathcal{D}_1 = \frac{1}{4} \sum_{i=1}^{n_1 - 1} \int_{x_i}^{x_{i+1}} W(x)[(x - x_i)(x - x_{i+1})]^2 [f''(\xi_i)]^2 \, dx. \tag{20}$$

Let $z_i = (x_i + x_{i+1})/2$, for $i = 1, 2, \cdots, n_1 - 1$. As n_1 becomes large and the lengths of the interpolation intervals approach zero, we can approximate $\mathcal{D}_1$ by

$$\begin{aligned} \mathcal{D}_1 &\approx \frac{1}{4} \sum_{i=1}^{n_1 - 1} \left(W(z_i)[f''(z_i)]^2 \right. \\ &\qquad \left. \times \int_{x_i}^{x_{i+1}} [(x - x_i)(x - x_{i+1})]^2 \, dx \right) \\ &= \frac{1}{120} \sum_{i=1}^{n_1 - 1} W(z_i)[f''(z_i)]^2 [\Delta x_i]^5 \end{aligned} \tag{21}$$

where $\Delta x_i = x_{i+1} - x_i$.

Now let the interpolation interval density function defined on the x axis be $\lambda_1(x)$. By its definition, we have

$$\lambda_1(z_i) \approx \frac{1}{(n_1 - 1)\Delta x_i} \tag{22}$$

for $i = 1, 2, \cdots, n_1 - 1$. Then, $\mathcal{D}_1$ in (21) can be further approximated by

$$\begin{aligned} \mathcal{D}_1 &\approx \frac{1}{120} \sum_{i=1}^{n_1 - 1} W(z_i)[f''(z_i)]^2 \frac{\Delta x_i}{(n_1 - 1)^4 [\lambda_1(z_i)]^4} \\ &\approx \frac{1}{120(n_1 - 1)^4} \int_A^B \frac{W(x)[f''(x)]^2}{[\lambda_1(x)]^4} \, dx. \end{aligned} \tag{23}$$

Applying Hölder's inequality [18], [26], we have

$$\begin{aligned} &\int_A^B \left(\frac{W(x)[f''(x)]^2}{[\lambda_1(x)]^4} \right)^{\frac{1}{5}} [\lambda_1(x)]^{\frac{4}{5}} \, dx \\ &\quad \le \left(\int_A^B \frac{W(x)[f''(x)]^2}{[\lambda_1(x)]^4} \, dx \right)^{\frac{1}{5}} \left(\int_A^B \lambda_1(x)\,dx \right)^{\frac{4}{5}}. \end{aligned} \tag{24}$$

From (18), we have

$$\int_A^B \frac{W(x)[f''(x)]^2}{[\lambda_1(x)]^4} \, dx \ge \left[\int_A^B \left(W(x)[f''(x)]^2 \right)^{\frac{1}{5}} dx \right]^5 \tag{25}$$

and the equality holds if

$$\frac{W(x)[f''(x)]^2}{[\lambda_1(x)]^4} = C\lambda_1(x) \tag{26}$$

for some constant C. Since the integral in the right hand side of (25) does not contain the design function $\lambda_1(x)$, it is a

lower bound of the integral in (23), and this lower bound can be achieved by choosing $\lambda_1(x)$ such that (26) is satisfied. Solving (26) for $\lambda_1(x)$ and choosing constant C to satisfy the constraint in (18), we obtain the optimal $\lambda_1(x)$ as

$$\lambda_1(x) = \frac{(W(x)[f''(x)]^2)^{\frac{1}{5}}}{\int_A^B (W(x)[f''(x)]^2)^{\frac{1}{5}}\,dx}. \tag{27}$$

The resulting minimum MSE for large n_1 is approximated by

$$\mathcal{D}_1^* \approx \frac{B_1}{120 n_1^4} \tag{28}$$

where

$$B_1 = \left[\int_A^B (W(x)[f''(x)]^2)^{\frac{1}{5}}\,dx\right]^5. \tag{29}$$

We see that the optimal grid point placement is determined by the second derivative of the function being interpolated. In the next subsection, we generalize this derivation to multidimensional functions.

D. Multidimensional SLI Design

For K-D, $K \geq 2$, SLI design, we define the number of partition grid points allocated to the x_1 axis within the finite interval $[A, B]$ to be n_1. For example, as shown in Fig. 4, $n_1 = 7$ partition grid points are allocated to the x_1 axis for a 3-D SLI. As also illustrated in the figure, each of these grid points corresponds to a $(K-1)$-D SLI structure, and we use $N_{K-1}(i)$, $i = 1, \cdots, n_1$, to denote the number of grid points to be allocated to the ith $(K-1)$-D SLI structure. The $N_{K-1}(i)$'s should satisfy the constraint

$$N_K = \sum_{i=1}^{n_1} N_{K-1}(i) \tag{30}$$

where N_K is the total number of interpolation grid points. In our example, we have $N_2(2) = 18$ and $N_2(6) = 20$. For the placement of grid points on the x_1 axis, we define the K-D interpolation interval density function $\lambda_K(x_1)$ similar to $\lambda_1(x)$ defined in (17) for the 1-D case. The objective of this subsection is to present closed form expressions for n_1, $\lambda_K(x_1)$, and $N_{K-1}(i)$, $i = 1, \cdots, n_1$, in the design of a K-D SLI. With these results, the $(K-1)$-D SLI grids may be allocated along the x_1 coordinate, and each of them can be designed by recursively applying this same procedure.

Before we can present the results, we need to define auxiliary functions $A_i(x_1, \cdots, x_{K-i})$ and $B_i(x_1, \cdots, x_{K-i})$ for $1 \leq i \leq K-1$. To motivate the definition of these functions, let us consider the $(i+1)$-D subspace in $(x_{K-i}, \cdots, x_K)$ with $x_1, \cdots, x_{K-i-1}$ fixed. To construct an $(i+1)$-D SLI structure in this subspace, we first place partition grid points on the x_{K-i} axis and then construct i-D SLI grid structures for the subspace in $(x_{K-i+1}, \cdots, x_K)$. Intuitively, we know that the MSE resulting from this $(i+1)$-D SLI can be divided into two parts: one from the interpolation error along the x_{K-i} direction and the other from the i-D SLI's for the subspace in $(x_{K-i+1}, \cdots, x_K)$. The function that affects the interpolation error along the x_{K-i} direction is the second partial derivative $\partial^2 f(\mathbf{x})/\partial x_{K-i}^2$, and for each x_{K-i}, it is summarized by

$$A_i(x_1, \ldots, x_{K-i}) = \int_{\Omega(x_1, \ldots, x_{K-i})} W(\mathbf{x}) \left(\frac{\partial^2 f(\mathbf{x})}{\partial x_{K-i}^2}\right)^2 dx_{K-i+1} \cdots dx_K \tag{31}$$

where $\Omega(x_1, \cdots, x_{K-i})$ denotes the restricted domain of $f(\mathbf{x})$ with $x_1, \cdots, x_{K-i}$ fixed. The function $B_i(x_1, \cdots, x_{K-i})$ is the MSE resulting from the i-D SLI with x_{K-i} fixed. From the recursive nature of the SLI design procedure, we know that the $B_i(x_1, \cdots, x_{K-i})$ can be defined recursively. Following the derivation presented in the Appendix, we define $B_i(x_1, \cdots, x_{K-i})$ by

$$B_i(x_1, \cdots, x_{K-i}) = \left(\int_{\Omega(x_1, \ldots, x_{K-i})} [A_{i-1}(x_1, \ldots, x_{K-i+1})]^{\frac{1}{i+4}} \times [B_{i-1}(x_1, \ldots, x_{K-i+1})]^{\frac{i-1}{i+4}}\, dx_{K-i+1}\right)^{\frac{i+4}{i}} \tag{32}$$

with the base of the recursion given by

$$B_1(x_1, \cdots, x_{K-1}) = \left[\int_{\Omega(x_1, \ldots, x_{K-1})} \left(W(\mathbf{x})\left[\frac{\partial^2 f(\mathbf{x})}{\partial x_K^2}\right]^2\right)^{\frac{1}{5}} dx_K\right]^5. \tag{33}$$

In the following, we give the formulas for $\lambda_K(x_1)$, n_1, and $N_{K-1}(i)$ for $i = 1, \cdots, n_1$, in terms of $A_{K-1}(x_1)$ and $B_{K-1}(x_1)$. The detailed derivations are given in the Appendix.

$$\lambda_K(x_1) \propto \left(\frac{[A_{K-1}(x_1)]^{K+3}}{[B_{K-1}(x_1)]^{K-1}}\right)^{\frac{1}{4K+16}} \tag{34}$$

$$n_1 = N_K^{1/K} \times \left(\frac{\int_A^B (A_{K-1}(x_1)/[\lambda_K(x_1)]^4)\,dx_1}{\left[\int_A^B [B_{K-1}(x_1)]^{\frac{K-1}{K+3}} [\lambda_K(x_1)]^{\frac{4}{K+3}}\,dx_1\right]^{\frac{K+3}{K-1}}}\right)^{\frac{K-1}{4K}} + 1 \tag{35}$$

where "$\propto$" denotes "proportional to."

Suppose that the n_1 partition grid points $x_1^{(i)}$, $1 \leq i \leq n_1$, are optimally positioned on the x_1 axis according to $\lambda_K(x_1)$ such that $A = x_1^{(1)} < x_1^{(2)} < \cdots < x_1^{(n_1)} = B$. The optimal number of grid points allocated to the ith $(K-1)$-D SLI structure can be approximated by

$$N_{K-1}(i) \approx \frac{N_K \left[B_{K-1}(x_1^{(i)})(z_1^{(i)} - z_1^{(i-1)})\right]^{\frac{K-1}{K+3}}}{\sum_{j=1}^{n_1} \left[B_{K-1}(x_1^{(j)})(z_1^{(j)} - z_1^{(j-1)})\right]^{\frac{K-1}{K+3}}} \tag{36}$$

where $z_1^{(0)} = A$, $z_1^{(n_1)} = B$, and $z_1^{(i)} = (x_1^{(i)} + x_1^{(i+1)})/2$ for $i = 1, 2, \cdots, n_1 - 1$.

```
Procedure Get_B_i(x_1, ..., x_{K-i}):

/* Obtain B_i(x_1, ..., x_{K-i}). */

if K > 1 then
    begin
        for each x^(j)_{K-i+1} do
            begin
                approximate A_{i-1}(x_1, ..., x^(j)_{K-i+1}) using (31);
                Get_B_{i-1}(x_1, ..., x^(j)_{K-i+1});
            end

        approximate B_i(x_1, ..., x_{K-i}) using (32);
    end
else
    begin
        calculate B_1(x_1, ..., x_K) using (40);
    end
```

Fig. 5. Pidgin ALGOL algorithm for calculating $B_i(x_1, \cdots, x_{K-i})$.

```
Procedure Asymptotic_SLI_Design(K, N_K):

/* K-D SLI design by asymptotic theory. */

if K > 1 then
    begin
        approximate A_{K-1}(x_1) using (31);
        Get_B_{K-1}(x_1);

        obtain λ_K(x_1) using (34);
        obtain n_1 using (35);

        position n_1 grid points on x_1 according to λ_K(x_1);

        for i ← 1 until n_1 do
            begin
                obtain N_{K-1}(i) using (36);
                Asymptotic_SLI_Design(K - 1, N_{K-1}(i));
            end
    end
else
    begin
        position N_1 grid points on x according to λ_1(x) in (27);
    end
```

Fig. 6. Pidgin ALGOL algorithm for the asymptotic SLI design procedure.

The resulting minimum MSE is given by

$$\mathcal{D}_K^* \approx \frac{KB_K}{120N_K^{4/K}} \tag{37}$$

where

$$B_K = \left(\int_A^B [A_{K-1}(x_1)]^{\frac{1}{K+4}} [B_{K-1}(x_1)]^{\frac{K-1}{K+4}} \, dx_1 \right)^{\frac{K+4}{K}}. \tag{38}$$

Equations (34)–(36) can guide us in optimally reducing a K-D SLI design problem into several independent $(K-1)$-D SLI design problems. In the next subsection, we will discuss how to use these formulas in practical applications.

E. Implementation Considerations

Since this paper deals with a design theory based on the asymptotic behavior of an interpolation structure as the number N of interpolation grid points approaches infinity, the function $f(\mathbf{x})$, $\mathbf{x} \in \mathbb{R}^K$, must be completely known for each $\mathbf{x}$ in the domain of the function; and $f(\mathbf{x})$ should be smooth in the sense that all of its second partial derivatives are continuous. However, in practical applications, these conditions are usually not satisfied. For example, in some cases the function and/or its partial derivatives may only be known at a set of discrete points.

In the application we present in Section V, the function to be interpolated is represented by a high-resolution uniform grid ($65 \times 65 \times 65$) and our objective is to design relatively low resolution (with number of grid points ranging from 9^3 to 17^3) SLI grid structures to approximate the original representation. Since our original function is itself represented by a discrete grid with only four to eight times the number of grid points for the objective low-resolution grid per dimension on average, we do not consider the smoothness condition of the asymptotic theory to be well satisfied. Here we present the detailed algorithm used for implementing (31)–(36) to design the SLI in our application. In the next section, we present a postprocessing technique that can improve on this design when the assumptions for the asymptotic analysis are not well satisfied.

Assume that the original function $f(\mathbf{x})$ is represented by a high-resolution uniform grid with the distance between adjacent grid points being h. To estimate the second partial derivatives $\partial^2 f(\mathbf{x})/\partial x_i^2$ on each grid point, we apply the standard numerical differentiation procedure, (39), shown at the bottom of the page. The integrals in (31)–(36) can be approximated by summations. For example, $B_1(x_1, \cdots, x_{K-1})$ in (33) can be approximated by

$$B_1(x_1, \cdots, x_{K-1}) \approx \left[\sum_{x_K^{(j)}} \left(W\left(x_1, \ldots, x_{K-1}, x_K^{(j)}\right) \times \left[\frac{\partial^2 f\left(x_1, \ldots, x_{K-1}, x_K^{(j)}\right)}{\partial x_K^2} \right]^2 \right)^{\frac{1}{5}} h \right]^5 \tag{40}$$

where $(x_1, \cdots, x_{K-1}, x_K^{(j)})$ denotes the set of grid points with $x_1, \cdots, x_{K-1}$ fixed. Since $B_i(x_1, \cdots, x_{K-i})$ is obtained recursively, we present the procedure for obtaining it in Fig. 5 as a Pidgin ALGOL algorithm. The complete K-D asymptotic SLI design procedure is given in Fig. 6.

$$\frac{\partial^2 f(\mathbf{x})}{\partial x_i^2} \approx \frac{f(x_1, \ldots, x_i - h, \cdots, x_K) - 2f(\mathbf{x}) + f(x_1, \cdots, x_i + h, \cdots, x_K)}{h^2} \tag{39}$$

IV. Postprocessing

The asymptotic analysis assumes that the number of interpolation grid points is large and the function to be interpolated is smooth. However, in practical applications, the number of interpolation grid points may not be very large and/or the function to be interpolated may not be very smooth. In this section, we develop a postprocessing technique to rearrange the grid points to further reduce the MSE. The postprocessing has two components: rearrangement of grid points on their respective axes and reallocation of grid points. Here, we assume that the original function is known at points on a uniform grid with much higher resolution than that of the SLI grid structure. We can evaluate the error in the approximation of $f(\mathbf{x})$ by the SLI structure at these high-resolution grid points and then use this information to estimate the overall MSE. We first discuss the rearrangement of grid points and then their reallocation. Finally, we present the overall postprocessing procedure. Similar ideas were applied to improve the design of SSQ resulting from the asymptotic theory [22].

A. Rearrangement of Grid Points

In the general K-D SLI structure, there are two kinds of grid points: the partition grid points that are placed on the $x_1, \cdots, x_{K-1}$ axes and the interpolation grid points that are placed on the x_K axis. There is no specific functional output mapped to a partition grid point since it actually specifies a subset in the domain of the function. Only the interpolation grid points are mapped to the functional outputs. For interpolation grid points on the x_K axis, since $x_1, \cdots, x_{K-1}$ are fixed, we can treat them the same as 1-D functions defined on the x_K axis. In this subsection, we use a 1-D function to present the procedure for rearrangement of interpolation grid points and then generalize the procedure to handle the rearrangement of partition grid points. The grid point rearrangement procedure presented here is a greedy algorithm. Its purpose is to reduce the error step by step until a local minimum is reached.

Suppose that the 1-D function $f(x)$ on $[A, B]$ is approximated by the n_1 point SLI implementation $\tilde{f}(x)$ initially designed according to the asymptotic theory. Assume that the n_1 grid points x_i, $1 \le i \le n_1$, are placed such that $A = x_1 < x_2 < \cdots < x_{n_1} = B$. We define the MSE on the ith interpolation interval, $1 \le i \le n_1 - 1$, as

$$\mathcal{E}_1(i) = \int_{x_i}^{x_{i+1}} W(x)[f(x) - \tilde{f}(x)]^2 \, dx. \tag{41}$$

To try to reduce the MSE resulting from $\tilde{f}(x)$, we first identify the interval $[x_m, x_{m+1}]$ such that $\mathcal{E}_1(m)$ is the maximum among the $\mathcal{E}_1(i)$'s for $i = 1, 2, \cdots, n_1 - 1$. Then as illustrated in Fig. 7, we move one of the nonboundary grid points x_j, where $j \neq 1, n_1$, to $x_o \in (x_m, x_{m+1})$, and optimally place it so that the overall MSE resulting from this new grid structure is minimized. Since the original function is represented by a high-resolution uniform grid, we can search the high-resolution grid points in (x_m, x_{m+1}) to find the optimal position for x_o. We note that the optimal position is the same for $j \neq m, m+1$ and can be predetermined. However, for $j = m$ or $m+1$, we need to redetermine the optimal position for x_o because in these situations one of the original boundaries of $[x_m, x_{m+1}]$ is removed. Among the $n_1 - 2$ new SLI structures resulting from moving x_j, $j = 2, \cdots, n_1 - 1$, we find the one which has the best MSE performance. If the MSE resulting from this SLI structure is not less than that from the original, we keep the original SLI structure and stop the grid point rearrangement process. Otherwise, we choose the new SLI structure and continue the grid point rearrangement process until no MSE improvement can be obtained.

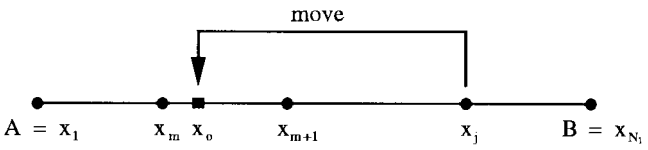

Fig. 7. Illustration of grid point rearrangement for postprocessing.

Now we generalize the procedure to handle partition grid points. Let us consider the rearrangement of grid points placed on the x_1 axis for a K-D SLI where $K \ge 2$. The main difficulty is that a partition grid point does not map to a functional output. However, we note from the discussions in Section III-B that the purpose of optimal placement of grid points on the x_1 axis is to minimize the MSE resulting from interpolation along the x_1 axis, assuming that the values used for interpolation are accurate. Since $\tilde{f}(x)$ is used to denote the interpolated function based on the SLI structure where the interpolation in the $(x_2, \cdots, x_K)$ subspace with x_1 fixed is not accurate, we need to define an intermediate function $\tilde{f}_I(\mathbf{x})$ to denote the interpolation along the x_1 axis with the assumption that the values used for the interpolation are accurate. Suppose that n_1 partition grid points $x_1^{(i)}$ are placed such that $x_1^{(1)} < x_1^{(2)} < \cdots < x_1^{(n_1)}$, then $\tilde{f}_I(\mathbf{x})$ is given by

$$\tilde{f}_I(\mathbf{x}) = \frac{f\big(x_1^{(i+1)}, x_2, \ldots, x_K\big) - f\big(x_1^{(i)}, x_2, \ldots, x_K\big)}{x_1^{(i+1)} - x_1^{(i)}} \times \big(x_1 - x_1^{(i)}\big) + f\big(x_1^{(i)}, x_2, \ldots, x_K\big) \tag{42}$$

for $x_1 \in [x_1^{(i)}, x_1^{(i+1)}]$, $i = 1, 2, \cdots, n_1 - 1$. Therefore, the MSE for the ith interval $[x_1^{(i)}, x_1^{(i+1)}]$ can be written as

$$\mathcal{E}_K(i) = \int_{x_1^{(i)}}^{x_1^{(i+1)}} \left(\int_{\Omega(x_1)} W(\mathbf{x}) \big[f(\mathbf{x}) - \tilde{f}_I(\mathbf{x})\big]^2 dx_2 \cdots dx_K \right) dx_1. \tag{43}$$

The objective of the partition grid rearrangement is to reduce $\mathcal{E}_K(i)$ in the equation above; and the procedure described earlier for rearrangement of interpolation grid points can readily be used for this purpose by replacing (41) by (43).

B. Reallocation of Grid Points

In K-D SLI designs where $K \ge 2$, we need to obtain n_1, the number of partition grid points to be placed on the x_1 axis, and $N_{K-1}(i)$, the number of grid points allocated for the $(K-1)$-D SLI structure corresponding to the ith partition grid point

on the x_1 axis for $i = 1, 2, \cdots, n_1$. These parameters can be obtained from the asymptotic design theory. However, if the assumptions for the asymptotic analysis are not well satisfied, we need to recompute these parameters using the actual MSE's resulting from the initial SLI structure designed according to the asymptotic theory.

We note from (36) of Section III-D that the $N_{K-1}(i)$'s depend on the error constants $B_{K-1}(x_1^{(i)})$. We see from (56) of the Appendix that the $B_{K-1}(x_1^{(i)})$'s are related to the MSE $\mathcal{D}_K^*$ resulting from the ith $(K-1)$-D SLI. Rearranging (56), we have

$$B_{K-1}(x_1^{(i)}) \approx \frac{120[N_{K-1}(i)]^{4/(K-1)}\mathcal{D}_{K-1}^*(x_1^{(i)})}{K-1} \tag{44}$$

where $N_{K-1}(i)$ is the number of grid points initially allocated to the ith $(K-1)$-D SLI. Applying this newly estimated $B_{K-1}(x_1^{(i)})$ to (36), we can obtain a new set of $N_{K-1}(i)$ from

$$N'_{K-1}(i) \approx \frac{N_K\left[\mathcal{D}_{K-1}^*(x_1^{(i)})[N_{K-1}(i)]^{4/(K-1)}\left(z_1^{(i)} - z_1^{(i-1)}\right)\right]^{\frac{K-1}{K+3}}}{\sum_{j=1}^{n_1}\left[\mathcal{D}_{K-1}^*(x_1^{(j)})[N_{K-1}(j)]^{4/(K-1)}\left(z_1^{(j)} - z_1^{(j-1)}\right)\right]^{\frac{K-1}{K+3}}}. \tag{45}$$

Equation (45) tells us that after a K-D SLI grid structure is obtained by the asymptotic theory, we can reduce the overall MSE by computing the actual MSE's for the $(K-1)$-D SLI's corresponding to the n_1 partition grid points placed on the x_1 axis, and using them to change number of grid points allocated to these $(K-1)$-D SLI's.

From (53) and (63) in the Appendix, we see that the integrals in (35) for the asymptotically optimal n_1 are related to $\mathcal{D}_K^{(1)}$ and $\mathcal{D}_K^{(2)}$, which correspond to the MSE's resulting from linear interpolation along the x_1 coordinate and the $(K-1)$-D SLI structures in the $(x_2, \cdots, x_K)$ space, respectively. Therefore, by expressing the integrals in (35) in terms of the actual MSE components estimated from the initial SLI structure designed according to the asymptotic theory, we can obtain a new n_1 from

$$n_1' = \left(\frac{(K-1)\mathcal{D}_K^{(1)}}{\mathcal{D}_K^{(2)}}\right)^{\frac{K-1}{4K}}(n_1 - 1) + 1 \tag{46}$$

where

$$\mathcal{D}_K^{(1)} \approx \sum_{i=1}^{n_1-1}\mathcal{E}_K(i) \tag{47}$$

and $\mathcal{D}_K^{(2)}$ is given by (55) in the Appendix. Here we see that after a K-D SLI grid structure is obtained by the asymptotic theory, we can reduce the overall MSE by computing actual MSE's resulting from the interpolation along the x_1 direction assuming the values used for interpolation are accurate, and computing the actual combined MSE from the $(K-1)$ SLI's. These MSE's are then used to modify the number n_1 of partition grid points allocated to the x_1 axis.

```
Procedure Postproc_SLI_Design(K, N_k):

/* K-D SLI design by asymptotic theory with post-processing. */

if K > 1 then
    for pass ← 1 until 2 do
        begin
            if pass = 1 then
                begin
                    approximate A_{K-1}(x_1) using (31);
                    Get_B_{K-1}(x_1);

                    obtain λ_K(x_1) using (34);
                    obtain n_1 using (35); /* asymptotic theory */
                end
            else
                begin
                    recompute n_1 using (46); /* based on current SLI */
                end

            position n_1 grid points on x_1 according to λ_K(x_1);
            rearrange grid points (Sec. 4.1);

            for i ← 1 until n_1 do
                begin
                    obtain N_{K-1}(i) using (36); /* asymptotic theory */
                    Postproc_SLI_Design(K - 1, N_{K-1}(i));
                end

            for i ← 1 until n_1 do
                begin
                    recompute N_{K-1}(i) using (45); /* based on current SLI */
                    Postproc_SLI_Design(K - 1, N_{K-1}(i));
                end
        end
else
    begin
        position N_1 grid points on x according to λ_1(x) in (27);
        rearrange grid points (Sec. 4.1);
    end
```

Fig. 8. Pidgin ALGOL algorithm for the overall postprocessing procedure.

C. Overall Procedure

The overall postprocessing procedure for designing a K-D SLI structure is given in Fig. 8 as a Pidgin ALGOL algorithm. This procedure is recursive. The design of a K-D SLI structure contains two passes. The first pass designs a K-D SLI structure with n_1 grid points allocated to the first axis where n_1 is obtained by the asymptotic theory. The second pass uses (46) to obtain a new n_1 and designs the final K-D SLI structure. Within each pass, we first use the asymptotic theory to position the n_1 grid points on the first axis and then use the procedure described in Section IV-A to rearrange them. Next we use the asymptotic theory to allocate $N_{K-1}(i)$'s to the $(K-1)$-D SLI's. In order to obtain a more accurate estimation of $N_{K-1}(i)$'s, we recursively apply the two-pass procedure to design these $(K-1)$-D SLI's. Then we use (45) to obtain the new $N_{K-1}(i)$'s and redesign the $(K-1)$-D SLI's.

V. Application to Color Printer Characterization and Calibration

In this section, we apply the SLI technique to the problem of color printer characterization and calibration, where highly nonlinear multidimensional functions have to be efficiently approximated. We first briefly introduce the printer characterization and calibration process and then present our experimental results.

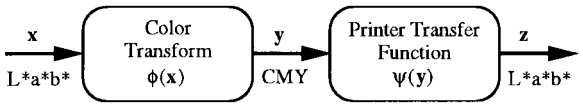

Fig. 9. Model for color printer characterization and calibration.

A. Color Printer Characterization and Calibration

The basic problem of printer characterization and calibration is illustrated in Fig. 9. Modern color management systems require that color printers be calibrated to some standard colorimetric space such as the CIE $L^*a^*b^*$ space [27]. To do this, we must first determine the printer transfer function $\psi(\mathbf{y})$, where $\mathbf{y}$ has the typical cyan, magenta, and yellow (CMY) components of printer colorants. This is the printer characterization process. Once $\psi(\mathbf{y})$ is determined, we implement a look-up table transformation to approximate its inverse $\phi(\mathbf{x}) = \psi^{-1}(\mathbf{x})$. In this way, the combined transfer function of the printer system is approximately unity, and output printer colors may be an accurate rendering of the input values $\mathbf{x}$. We note that the transfer function of a typical color printer is highly nonlinear, due to the interaction of the printer colorants and paper substrate. The details of the color printer characterization and calibration process are described in [8], and some of the recent approaches to interpolating color data are presented in [28] and [29].

The conventional approach [9], [10] to the color printer characterization and calibration problem is to first uniformly sample the printer input (CMY) space and, in the CIE $L^*a^*b^*$ space, measure the printer output at these sample points. Trilinear interpolation based on these measured points is then used to approximate the printer transfer function $\psi(\mathbf{y})$. To approximate the inverse printer transfer function $\phi(\mathbf{x})$, we uniformly sample the CIE $L^*a^*b^*$ space and obtain the corresponding CMY vectors at these sample points by applying inverse tetrahedral linear interpolation [9], [10] to the forward measurement data. Trilinear interpolation based on this data set is then used to approximate $\phi(\mathbf{x})$.

Instead of using the conventional approach, we can apply the SLI technique to both the printer characterization and calibration processes. When it is applied to the printer characterization process, we can use the same number of measurement points in the printer input (CMY) space to achieve a better approximation of $\psi(\mathbf{y})$ in terms of MSE than is possible with a uniform grid. Similarly, when applied to the calibration process, we can use the same number of interpolation grid points to achieve a better approximation of $\phi(\mathbf{x})$ in terms of the error between the input vector $\mathbf{x}$ and the printed output vector $\mathbf{z}$ in the CIE $L^*a^*b^*$ space. We have applied the SLI technique to approximate the inverse printer transfer function $\phi(\mathbf{x})$ and the results are reported in [30]–[32]. In this section, we present results for applying the SLI technique to the printer characterization process.

B. Experimental Results

We applied the SLI technique to approximate the printer transfer function obtained from a model [33] for a Xerox color printer. We used a high-resolution data set generated from the printer model. In this data set, the printer input (CMY) space is sampled on a $65 \times 65 \times 65$ uniform grid; and for each sample point the simulated printer output vector in the CIE $L^*a^*b^*$ space is calculated from the model. The domain of this printer transfer function is a cube where the C, M, and Y values range from zero to 255. At the printer output, L^* ranges from 9 to 96, a^* ranges from -62 to 80, and b^* ranges from -65 to 100. In this experiment, we show that if a smaller number of grid points are used to approximate the original data set, the appropriately designed SLI structure can greatly reduce the mean squared approximation error. We present results for 1-D, 2-D, and 3-D cases based on this data set.

For 1-D interpolation, we let $C = 20$, $M = 64$, and obtain a 1-D functional relationship between the output a^* value and input Y value from the original data set. We use nine interpolation grid points to approximate the original 65-point functional data, and implement the interpolation using the uniform grid and the SLI grid designed by the asymptotic theory with postprocessing. The grid point placements for the uniform and the SLI grids are shown in Fig. 10 and the error distributions resulting from them in Fig. 11. From Figs. 10(a) and 11(a), we see that the function is very nonlinear in the interval (200, 255) and most of the error for the uniform grid interpolation occurs in this interval. From Figs. 10(b) and 11(b), we observe that in the SLI structure, more grid points are allocated to this interval and the error is smaller and more evenly distributed than that resulting from the uniform grid.

To obtain a 2-D function of L^* in terms of M and Y, we let $C = 0$. An SLI interpolation structure is designed to approximate this function using 9^2 interpolation grid points. Fig. 12 shows the grid structures for the uniform grid and the SLI grid obtained by postprocessing. The error distributions resulting from these structures are shown in Fig. 13. From these figures, we see that in the SLI grid, many grid lines are placed on the M axis in the interval (200, 255). However, there are only two to three grid points allocated to these grid lines. This shows that in this region, most of the nonlinearity of the function is oriented along the M-axis. The error distribution resulting from the SLI grid is much smaller and more evenly distributed than that resulting from the uniform grid.

Finally, we decompose the Xerox data set into three scalar-valued functions with L^*, a^*, and b^* as output values, respectively. The different interpolation schemes are used to approximate these scalar-valued 3-D functions. Here, we present in Fig. 14 the results for the combined root mean squared (RMS) ΔE performance for each grid structure where ΔE is defined by

$$\Delta E = \sqrt{(\Delta L^*)^2 + (\Delta a^*)^2 + (\Delta b^*)^2}. \tag{48}$$

From this figure, we observe that we can reduce the RMS error by at least three to four times with an SLI structure designed by postprocessing. We see that if the average number of grid points per dimension is greater than nine, the SLI structure designed by the asymptotic theory provides most of the error reduction. However, when the number of grid points is small, the SLI structure designed by the asymptotic theory is not very effective and most of the error reduction is provided by postprocessing.

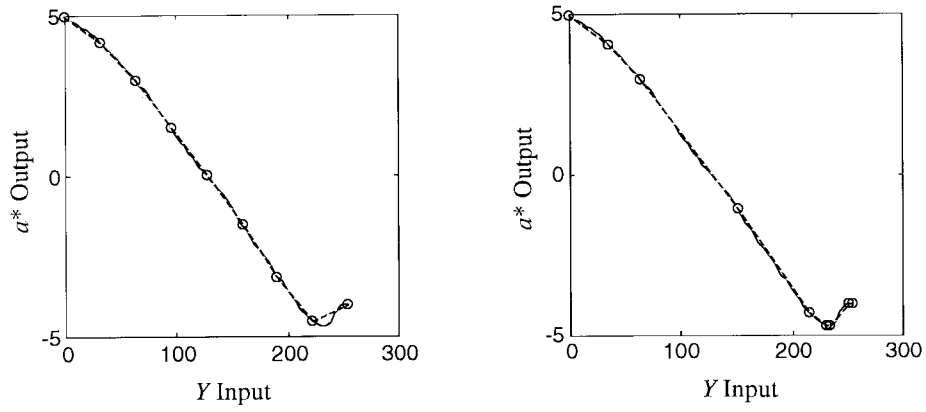

Fig. 10. One-dimensional grid point placement for (a) nine-point uniform grid and (b) nine-point SLI grid designed by postprocessing. The grid points are superimposed on the original function which is represented by the solid curve and the approximated function is represented by the dashed line segments connecting the grid points.

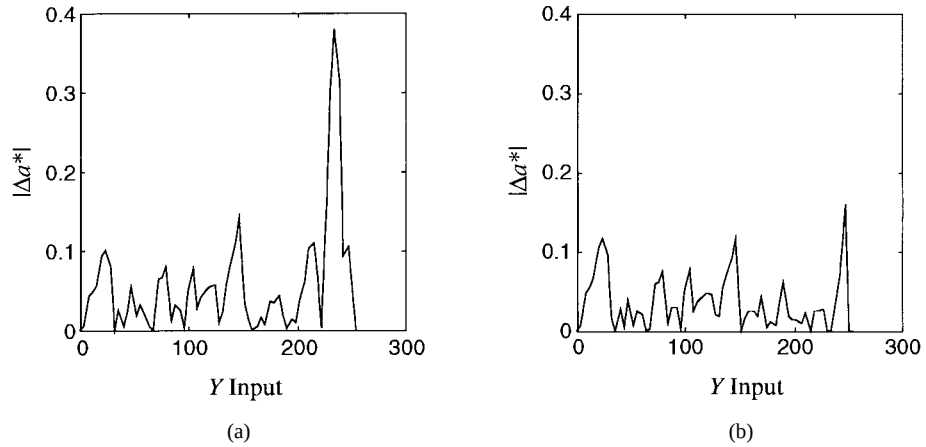

Fig. 11. One-dimensional error distribution for (a) nine-point uniform grid and (b) nine-point SLI grid designed by the postprocessing technique.

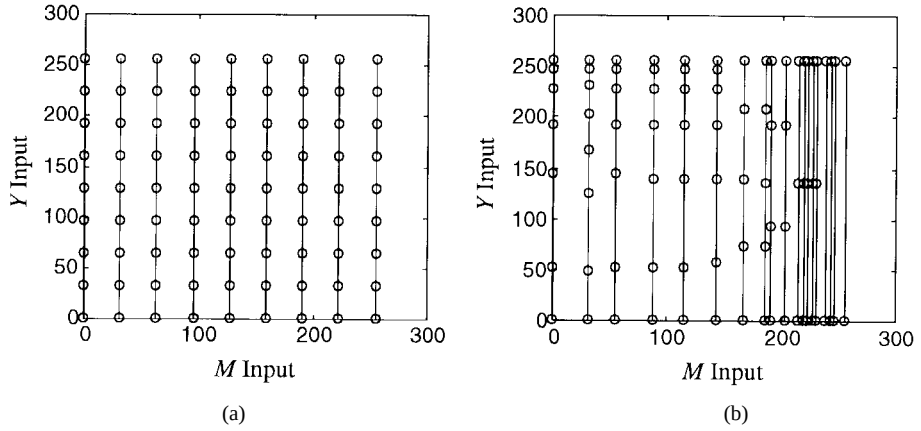

Fig. 12. Two-dimensional grid point placement for (a) 9^2-point uniform grid and (b) 9^2-point SLI grid designed by the postprocessing technique.

VI. Conclusion

In this paper, we considered the problem of finding the optimal interpolation scheme to approximate a multidimensional nonlinear function using a finite number of interpolation grid points. We developed an asymptotic theory of optimal functional approximation based on the SLI grid structure where the approximating functions are multidimensional linear splines. In the asymptotic theory, optimal values for the SLI design parameters are expressed in terms of the second partial derivatives of the function to be interpolated.

The asymptotic analysis not only provides intuition about the behavior of the SLI, but can also serve as a valuable guide

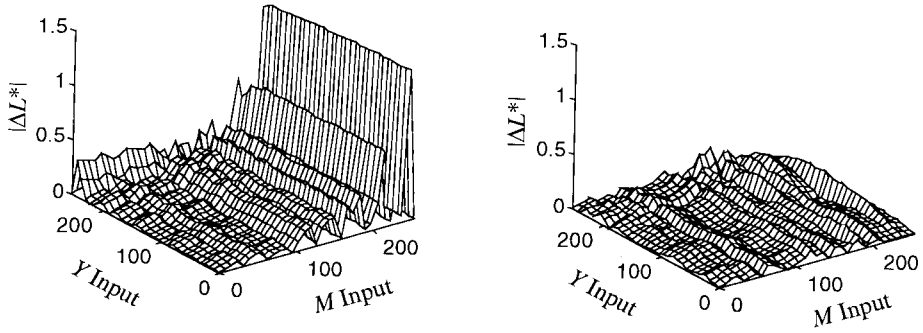

Fig. 13. Two-dimensional error distribution for (a) 9^2-point uniform grid and (b) 9^2-point SLI grid designed by the postprocessing technique.

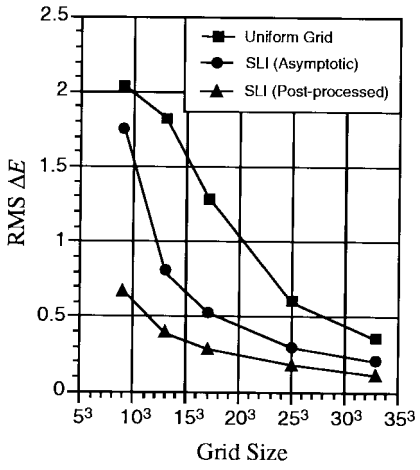

Fig. 14. RMS ΔE performance for 3-D interpolations.

in the design of the SLI grid structures even if the number of grid points is small. To further improve the MSE performance of the SLI structure, we developed a postprocessing technique to fine-tune the grid point placement when the assumptions for the asymptotic analysis are not well satisfied.

We applied the SLI technique to approximate a very nonlinear color printer transfer function. Our experimental results showed that by using the appropriately designed SLI structure, we can significantly improve the MSE performance over the conventional uniform grid.

Appendix
Multidimensional Asymptotic Analysis

The objective of this appendix is to show that (34)–(38) presented in Section III-D are valid. From the discussions in Section III, we see that the SLI design process is recursive. Here, we will show that if a K-D, $K \geq 2$, SLI structure with N_K grid points is recursively reduced to 1-D SLI's using the formulas (34)–(36) and the 1-D SLI's are designed using (27) in Section III-C, then the MSE resulting from the K-D SLI is minimum and is given by (37)–(38). From (28) of Section III-C, we see that (37) is valid for $K = 1$ where B_1 is given by (29). We will use mathematical induction to show that (37)–(38) are valid for $K \geq 2$.

In order to reduce a K-D SLI into $(K-1)$-D SLI's, we divide the MSE $\mathcal{D}_K$ in (15) into two parts, as follows:

$$\mathcal{D}_K = \mathcal{D}_K^{(1)} + \mathcal{D}_K^{(2)} \tag{49}$$

where $\mathcal{D}_K^{(1)}$ and $\mathcal{D}_K^{(2)}$ correspond to the MSE's introduced by the linear interpolation along the x_1 axis and by the $(K-1)$-D SLI structures in the $(x_2, \cdots, x_K)$ space, respectively. They are given by

$$\mathcal{D}_K^{(1)} = D_1, \tag{50}$$

and

$$\mathcal{D}_K^{(2)} = \sum_{i=2}^{K} D_i \tag{51}$$

where the D_i's are defined in (16).

We see from (16) that $\mathcal{D}_K^{(1)}$ is the weighted integral of $\Delta f_1(\mathbf{x})$, which is the error resulting from linear interpolation along the x_1 coordinate. Suppose that the n_1 partition grid points $x_1^{(i)}$, $1 \leq i \leq n_1$, are placed on the x_1 axis such that $A = x_1^{(1)} < x_1^{(2)} < \cdots < x_1^{(n_1)} = B$. Similar to (19) in Section III-C, $\Delta f_1(\mathbf{x})$ for $x_1 \in [x_1^{(i)}, x_1^{(i+1)}]$ can be expressed as

$$\Delta f_1(\mathbf{x}) = \frac{1}{2}\left(x_1 - x_1^{(i)}\right)\left(x_1 - x_1^{(i+1)}\right)\frac{\partial^2 f\left(\xi_1^{(i)}, x_2, \cdots, x_K\right)}{\partial x_1^2} \tag{52}$$

where $\xi_1^{(i)} \in [x_1^{(i)}, x_1^{(i+1)}]$ and in general depends on x_1. Following the procedure for deriving (23) in Section III-C, we can obtain

$$\mathcal{D}_K^{(1)} \approx \frac{1}{120(n_1-1)^4}\int_A^B \frac{A_{K-1}(x_1)}{[\lambda_K(x_1)]^4}\,dx_1. \tag{53}$$

Since $\mathcal{D}_K^{(2)}$ does not depend on $\Delta f_1(\mathbf{x})$, we rewrite it as

$$\mathcal{D}_K^{(2)} = \int_A^B \left(\sum_{i=2}^{K}\int_{\Omega(x_1)} W(\mathbf{x})[\Delta f_i(\mathbf{x})]^2\,dx_2\cdots,dx_K\right)dx_1. \tag{54}$$

Here, we observe that if $x_1 = x_1^{(i)}$, $i = 1, \cdots, n_1$, then the integrand of the outer integral is the MSE $\mathcal{D}_{K-1}(x_1^{(i)})$ of the $(K-1)$-D SLI located at partition grid point $x_1^{(i)}$. Let $z_1^{(0)} = A$, $z_1^{(n_1)} = B$, and $z_1^{(i)} = (x_1^{(i)} + x_1^{(i+1)})/2$ for $i = 1, 2, \cdots, n_1 - 1$, as presented in Section III-D. Now we

assume that asymptotically the number of grid points on the x_1 axis becomes very large and the interpolation intervals become very small. Therefore, the distance between consecutive $z_1^{(i)}$'s will become very small, and we can approximate the outer integral in (54) by a summation

$$\mathcal{D}_K^{(2)} \approx \sum_{i=1}^{n_1} \mathcal{D}_{K-1}\big(x_1^{(i)}\big)\big(z_1^{(i)} - z_1^{(i-1)}\big). \tag{55}$$

Suppose that $N_{K-1}(i)$ is the number of interpolation grid points allocated to the $(K-1)$-D SLI located at $x_1^{(i)}$. Now we assume that the $(K-1)$-D SLI's are optimally designed according to the asymptotic theory and the results in Section III-D are valid for $(K-1)$-D SLI's. By comparing (32) for $i = K-1$ and (38) in Section III-D, we see that the $B_{K-1}(x_1^{(i)})$ defined in (32) is the error constant for the ith $(K-1)$-D SLI. Therefore, the minimum $\mathcal{D}_{K-1}(x_1^{(i)})$ is given by

$$\mathcal{D}_{K-1}^{*}\big(x_1^{(i)}\big) \approx \frac{(K-1)B_{K-1}\big(x_1^{(i)}\big)}{120[N_{K-1}(i)]^{4/(K-1)}}. \tag{56}$$

Substituting this into (55), we have

$$\mathcal{D}_K^{(2)} \approx \frac{K-1}{120}\sum_{i=1}^{n_1} \frac{B_{K-1}\big(x_1^{(i)}\big)\big(z_1^{(i)} - z_1^{(i-1)}\big)}{[N_{K-1}(i)]^{4/(K-1)}} \tag{57}$$

assuming that the $(K-1)$-D SLI's are optimally designed according to the asymptotic theory. We apply the discrete version of Hölder's inequality [26] to obtain

$$\begin{aligned}
&\sum_{i=1}^{n_1}\left[\frac{B_{K-1}\big(x_1^{(i)}\big)\big(z_1^{(i)} - z_1^{(i-1)}\big)}{[N_{K-1}(i)]^{4/(K-1)}}\right]^{\frac{K-1}{K+3}} [N_{K-1}(i)]^{\frac{4}{K+3}} \\
&\quad \le \left(\sum_{i=1}^{n_1}\frac{B_{K-1}\big(x_1^{(i)}\big)\big(z_1^{(i)} - z_1^{(i-1)}\big)}{[N_{K-1}(i)]^{4/(K-1)}}\right)^{\frac{K-1}{K+3}} \\
&\qquad \times \left[\sum_{i=1}^{n_1} N_{K-1}(i)\right]^{\frac{4}{K+3}}.
\end{aligned} \tag{58}$$

Applying (30), we have

$$\begin{aligned}
&\sum_{i=1}^{n_1}\frac{B_{K-1}\big(x_1^{(i)}\big)\big(z_1^{(i)} - z_1^{(i-1)}\big)}{[N_{K-1}(i)]^{4/(K-1)}} \\
&\quad \ge \frac{1}{N_K^{4/(K-1)}}\left(\sum_{i=1}^{n_1}\big[B_{K-1}\big(x_1^{(i)}\big)\big(z_1^{(i)} - z_1^{(i-1)}\big)\big]^{\frac{K-1}{K+3}}\right)^{\frac{K+3}{K-1}}
\end{aligned} \tag{59}$$

and the equality holds if

$$\frac{B_{K-1}\big(x_1^{(i)}\big)\big(z_1^{(i)} - z_1^{(i-1)}\big)}{[N_{K-1}(i)]^{4/(K-1)}} = C_1 N_{K-1}(i) \tag{60}$$

for $i = 1, 2, \ldots, n_1$, and a constant C_1. Therefore, we have

$$\begin{aligned}
\mathcal{D}_K^{(2)} &\ge \frac{(K-1)}{120N_K^{4/(K-1)}} \\
&\quad \times \left(\sum_{i=1}^{n_1}\big[B_{K-1}\big(x_1^{(i)}\big)\big(z_1^{(i)} - z_1^{(i-1)}\big)\big]^{\frac{K-1}{K+3}}\right)^{\frac{K+3}{K-1}} \\
&= \frac{(K-1)}{120N_K^{4/(K-1)}}\left[\sum_{i=1}^{n_1}\frac{\big[B_{K-1}\big(x_1^{(i)}\big)\big]^{\frac{K-1}{K+3}}}{\big(z_1^{(i)} - z_1^{(i-1)}\big)^{\frac{4}{K+3}}}\right. \\
&\quad \left. \times \big(z_1^{(i)} - z_1^{(i-1)}\big)\right]^{\frac{K+3}{K-1}}.
\end{aligned} \tag{61}$$

By the definition of $\lambda_K(x_1)$, we have

$$z_1^{(i)} - z_1^{(i-1)} \approx \frac{1}{(n_1-1)\lambda_K\big(x_1^{(i)}\big)}. \tag{62}$$

Substituting this into (61), we obtain

$$\begin{aligned}
\mathcal{D}_K^{(2)} &\ge \frac{(K-1)(n_1-1)^{4/(K-1)}}{120N_K^{4/(K-1)}}\left[\sum_{i=1}^{n_1}\big[B_{K-1}\big(x_1^{(i)}\big)\big]^{\frac{K-1}{K+3}}\right. \\
&\quad \left. \times \big[\lambda_K\big(x_1^{(i)}\big)\big]^{\frac{4}{K+3}}\big(z_1^{(i)} - z_1^{(i-1)}\big)\right]^{\frac{K+3}{K-1}} \\
&\approx (K-1)\left[\frac{(n_1-1)^4}{120N_K^4}\left(\int_A^B [B_{K-1}(x_1)]^{\frac{K-1}{K+3}}\right.\right. \\
&\quad \left.\left. \times [\lambda_K(x_1)]^{\frac{4}{K+3}}\,dx_1\right)^{(K+3)}\right]^{\frac{1}{K-1}}.
\end{aligned} \tag{63}$$

Therefore, we have

$$\begin{aligned}
\mathcal{D}_K &\ge \frac{1}{120(n_1-1)^4}\int_A^B \frac{A_K(x_1)}{[\lambda_K(x_1)]^4}\,dx_1 \\
&\quad + (K-1)\left[\frac{(n_1-1)^4}{120N_K^4}\left(\int_A^B [B_{K-1}(x_1)]^{\frac{K-1}{K+3}}\right.\right. \\
&\quad \left.\left. \times [\lambda_K(x_1)]^{\frac{4}{K+3}}\,dx_1\right)^{(K+3)}\right]^{\frac{1}{K-1}}.
\end{aligned} \tag{64}$$

Applying the inequality for weighted means [26] to the right hand side of (64), we can obtain

$$\begin{aligned}
\mathcal{D}_K &\ge \frac{K}{120N_K^{4/K}}\left(\left[\int_A^B \frac{A_K(x_1)}{[\lambda_K(x_1)]^4}\,dx_1\right]^{\frac{1}{K+4}}\right. \\
&\quad \left. \times \left[\int_A^B [B_{K-1}(x_1)]^{\frac{K-1}{K+3}}[\lambda_K(x_1)]^{\frac{4}{K+3}}\,dx_1\right]^{\frac{K+3}{K+4}}\right)^{\frac{K+4}{K}}
\end{aligned} \tag{65}$$

and the equality holds if the constraint

$$\frac{1}{120(n_1-1)^4}\int_A^B \frac{A_K(x_1)}{[\lambda_K(x_1)]^4}\,dx_1 = \frac{(n_1-1)^{4/(K-1)}}{120N_K^{4/(K-1)}} \times \left[\int_A^B [B_{K-1}(x_1)]^{\frac{K-1}{K+3}}[\lambda_K(x_1)]^{\frac{4}{K+3}}\,dx_1\right]^{\frac{K+3}{K-1}} \tag{66}$$

is satisfied. Applying Hölder's inequality to the right-hand side of (65), we have

$$\mathcal{D}_K \geq \frac{K}{120N_K^{4/K}} \times \left(\int_A^B [A_K(x_1)]^{\frac{1}{K+4}}[B_K(x_1)]^{\frac{K-1}{K+4}}\,dx_1\right)^{\frac{K+4}{K}} \tag{67}$$

and the equality holds if the constraint

$$\frac{A_K(x_1)}{[\lambda_K(x_1)]^4} = C_2[B_{K-1}(x_1)]^{\frac{K-1}{K+3}}[\lambda_K(x_1)]^{\frac{4}{K+3}} \tag{68}$$

is satisfied for some constant C_2.

We see that the right-hand side of (67) does not contain the K-D SLI design parameters and functions. So it is a lower bound for $\mathcal{D}_K$ in (49). In order for this lower bound to become the minimum of $\mathcal{D}_K$, the equalities in (59), (65), and (67) have to hold simultaneously. Therefore, the constraints in (60), (66), and (68) must be satisfied simultaneously. Solving (68), (66), and (60), we obtain the optimal K-D SLI design criteria (34)–(36) in Section III-D. By comparing (67) with (37)–(38) in Section III-D, we see that (37) is the minimum of $\mathcal{D}_K$. Therefore, we have recursively shown that (34)–(38) in Section III-D are valid for $K \geq 2$.

ACKNOWLEDGMENT

The authors acknowledge helpful discussions with the personnel at Apple Computer, Inc., during the course of this research project, and Dr. R. Balasubramanian of Xerox Corporation for providing us the printer simulation data for our experiment.

REFERENCES

[1] J. Zhong, R. J. Adrian, and T. S. Huang, "Interpolation of multidimensional random processes with application to fluid flow," in *Proc. 1993 Int. Conf. Acoustics, Speech, and Signal Processing*, Minneapolis, MN, April 1993, vol. V, pp. 181–184.

[2] B. Hamann and J.-L. Chen, "Data point selection for piecewise linear curve approximation," *Comput. Aided Geometric Design*, vol. 11, pp. 289–301, June 1994.

[3] F. Lu and E. E. Milios, "Optimal local spline approximation of planar shape," in *Proc. 1991 Int. Conf. Acoustics, Speech, and Signal Processing*, Toronto, Ont., Canada, May 1991, vol. 4, pp. 2469–2472.

[4] ———, "Optimal spline fitting to planar shape," *Signal Process.*, vol. 37, pp. 129–140, May 1994.

[5] Y. Sato, "Piecewise linear approximation of plane curves by perimeter optimization," *Pattern Recognit.*, vol. 25, pp. 1535–1543, Dec. 1992.

[6] F. L. Kitson, "An algorithm for curve and surface fitting using B-splines," in *Proc. 1989 Int. Conf. Acoustics, Speech, and Signal Processing*, Glasgow, Scotland, May 1989, vol. 2, pp. 1207–1210.

[7] I. Qamar, "Method to determine optimum number of knots for cubic splines," *Commun. Numer. Methods Eng.*, vol. 9, pp. 483–488, Sept. 1993.

[8] M. C. Stone, W. B. Cowan, and J. C. Beatty, "Color gamut mapping and the printing of digital color images," *ACM Trans. Graph.*, vol. 7, pp. 249–292, Oct. 1988.

[9] S. I. Nin, J. M. Kasson, and W. Plouffe, "Printing CIELAB images on a CMYK printer using tri-linear interpolation," in *Proc. SPIE*, San Jose, CA, Feb. 1992, vol. 1670, pp. 316–324.

[10] P.-C. Hung, "Colorimetric calibration in electronic imaging devices using a look-up-table model and interpolations," *J. Electron. Imaging*, vol. 2, pp. 53–61, Jan. 1993.

[11] A. Cantoni, "Optimal curve fitting with piecewise linear functions," *IEEE Trans. Comput.*, vol. C-20, pp. 59–67, Jan. 1971.

[12] T. Pavlidis, "Optimal piecewise polynomial L_2 approximation of functions of one and two variables," *IEEE Trans. Comput.*, vol. C-24, pp. 98–102, Jan. 1975.

[13] ———, "Polygonal approximations by Newton's method," *IEEE Trans. Comput.*, vol. C-26, pp. 800–807, Aug. 1977.

[14] N. N. Abdelmalek, "Piecewise linear least-squares approximation of planar curves," *Int. J. Syst. Sci.*, vol. 21, pp. 1393–1403, July 1990.

[15] G. F. Carey and H. T. Dinh, "Grading functions and mesh redistribution," *SIAM J. Numer. Anal.*, vol. 22, pp. 1028–1040, Oct. 1985.

[16] M. J. Baines, "Algorithms for optimal discontinuous piecewise linear and constant L_2 fits to continuous functions with adjustable nodes in one and two dimensions," *Math. Computat.*, vol. 62, pp. 645–669, Apr. 1994.

[17] S. Na and D. L. Neuhoff, "Bennett's integral for vector quantizers," *IEEE Trans. Inform. Theory*, vol. 41, pp. 886–900, July 1995.

[18] A. Gersho and R. M. Gray, *Vector Quantization and Signal Compression*. Norwell, MA: Kluwer, 1991, chs. 5, 10.

[19] A. Gersho, "Asymptotically optimal block quantization," *IEEE Trans. Inform. Theory*, vol. IT-25, pp. 373–380, July 1979.

[20] A. U. Ağar, J. P. Allebach, and C. A. Bouman, "Minimax methods for surface interpolation using an SLI structure," in *Proc. 9th IEEE/IS&T Workshop on Image and Multidimensional Signal Processing*, Belize City, Belize, Mar. 1996, pp. 66–67.

[21] R. Balasubramanian, C. A. Bouman, and J. P. Allebach, "Sequential scalar quantization of vectors: An analysis," *IEEE Trans. Image Processing*, vol. 4, pp. 1282–1295, Sept. 1995.

[22] ———, "Sequential scalar quantization of color images," *J. Electron. Imaging*, vol. 3, pp. 45–59, 1994.

[23] J. Z. Chang and J. P. Allebach, "Optimal sequential scalar quantization of vectors," in *Proc. 27th Asilomar Conf. Signals, Systems, and Computers*, Pacific Grove, CA, Nov. 1993, pp. 265–271.

[24] J. Z. Chang, "Sequential structures for vector quantization and functional approximation," Ph.D. dissertation, School Electr. Eng., Purdue Univ., West Lafayette, IN, May 1995.

[25] S. D. Conte and C. de Boor, *Elementary Numerical Analysis: An Algorithmic Approach*, 3rd ed. New York: McGraw-Hill, 1980. chapter 2.

[26] G. H. Hardy, J. E. Littlewood, and G. Pólya, *Inequalities*, 2nd ed. Cambridge, U.K.: Cambridge Univ. Press, 1952, chapter 2.

[27] R. S. Gentile, "Device independent color in PostScript," in *Proc. SPIE*, San Jose, CA, Feb. 1993, vol. 1913, pp. 419–432.

[28] I. E. Bell and W. Cowan, "Characterizing printer gamut using tetrahedral interpolation," in *Proc. 1st IS&T/SID Color Imaging Conf.*, Scottsdale, AZ, Nov. 1993, pp. 108–113.

[29] S. A. Rajala and A. P. Kakodkar, "Interpolation of color data," in *Proc. 1st IS&T/SID Color Imaging Conf.*, Scottsdale, AZ, Nov. 1993, pp. 180–183.

[30] J. P. Allebach, J. Z. Chang, and C. A. Bouman, "Efficient implementation of nonlinear color transformations," in *Proc. 1st IS&T/SID Color Imaging Conf.*, Scottsdale, AZ, Nov. 1993, pp. 143–148.

[31] J. Z. Chang, C. A. Bouman, and J. P. Allebach, "Recent results in color calibration using sequential linear interpolation," in *Proc. ICPS'94/IS&T's 47th Ann. Conf.*, Rochester, NY, May 1994, vol. 2, pp. 500–505.

[32] J. Z. Chang, J. P. Allebach, and C. A. Bouman, "Optimal sequential linear interpolation applied to nonlinear color transformations," in *Proc.1st IEEE Int. Conf. Image Processing*, Austin, TX, Nov. 1994, vol. 3, pp. 987–990.

[33] R. Rolleston and R. Balasubramanian, "Accuracy of various types of Neugebauer model," in *Proc. 1st IS&T/SID Color Imaging Conf.*, Scottsdale, AZ, Nov. 1993, pp. 32–37.

James Z. Chang (SM'89–M'95) received the B.S. degree in electrical engineering from the South China Institute of Technology, Guangzhou, China, in 1986, the M.S. degree in applied mathematics from Oakland University, Rochester, MI, in 1988, and the Ph.D. degree in electrical engineering from Purdue University, West Lafayette, IN, in 1995.

He joined Color Savvy Systems Incorporated, Springboro, OH, in 1994, where he is now a Senior Scientist. He is responsible for developing advanced algorithms for the calibration of various color imaging devices in electronic imaging systems. His research interests include signal processing, image processing, and the application of color science and technology to electronic imaging. He is particularly interested in image processing techniques related to the scanning, storage, transmission, display, and printing of color images.

Dr. Chang is a member of SPIE, the Society for Imaging Science and Technology (IS&T), Eta Kappa Nu, and Tau Beta Pi.

Jan P. Allebach (S'70–M'76–SM'89–F'91) received the B.S. degree from the University of Delaware, Newark, in 1972, and the M.S. and Ph.D. degrees from Princeton University, Princeton, NJ, in 1975 and 1976, respectively, all in electrical engineering.

From 1972 to 1975, he was a National Science Foundation Graduate Fellow. He was with the Department of Electrical Engineering, University of Delaware, from 1976 to 1983. Since 1983, he has been with the School of Electrical and Computer Engineering, Purdue University, where he holds the rank of Professor. He has been a visiting summer faculty member at the IBM T. J. Watson Research Center, Yorktown Heights, NY, Sandia Labs, Livermore, CA, and Hewlett-Packard Labs, Palo Alto, CA. In addition, he has consulted extensively for industry and government laboratories. His research has primarily been in the areas of printing and display of images, scanning and sampling of multidimensional signals, and synthesis of digital diffractive elements.

Prof. Allebach is a Fellow of the Society for Imaging Science and Technology (IS&T), and a member of the Optical Society of America. In 1987, he received the Senior Award from the IEEE Signal Processing Society for his paper on time-sequential sampling published in the February 1984 issue of the IEEE TRANSACTIONS ON SIGNAL PROCESSING. During 1991–1992, he served as the IS&T Visiting Lecturer. During 1994–1995, he was a Distinguished Lecturer for the IEEE Signal Processing Society. He received an Outstanding Engineering Alumni Award from the University of Delaware in 1996. He has also received two teaching awards at Purdue University, West Lafayette, IN. He served on the Image and Multidimensional Signal Processing (IMDSP) Technical Committee of the IEEE Signal Processing Society from 1986 to 1995, and chaired it from 1991 to 1992. He served as Secretary of the IEEE Signal Processing Society from 1992 to 1995. Presently, he is serving as an elected member of the IEEE Signal Processing Society Board of Governors. He served as Chapters Vice President of IS&T from 1992 to 1996. He is a past Associate Editor for the IEEE TRANSACTIONS ON SIGNAL PROCESSING. During 1992–1994, he served on the Editorial Board for the *Journal of Electronic Imaging*. He was Technical Co-Chair of ICASSP-93 held in Minneapolis, MN, and General Co-Chair of the 9th IMDSP Workshop held in Belize City, Belize, in March 1996.

Charles A. Bouman (M'89) received the B.S.E.E. degree from the University of Pennsylvania, Philadelphia, in 1981, and the M.S. degree in electrical engineering from the University of California, Berkeley, in 1982. In 1987 and 1989, respectively, he received the M.A. and Ph.D. degrees in electrical engineering from Princeton University under the support of an IBM graduate fellowship.

From 1982 to 1985, he was a staff member in the Analog Device Technology Group at the Lincoln Laboratory, Massachusetts Institute of Technology, Cambridge. In 1989, he joined the faculty of Purdue University, West Lafayette, IN, where he currently holds the position of Associate Professor in the School of Electrical and Computer Engineering. His research interests include statistical image modeling and analysis, multiscale processing, and the display and printing of images. He is particularly interested in the applications of statistical signal processing techniques to problems such as fast image search and inspection, tomographic reconstruction, and document segmentation. He has performed research for numerous government and industrial organizations, including the National Science Foundation, the U.S. Army, Hewlett-Packard, NEC Corporation, Apple Computer, Xerox, and Eastman Kodak. From 1991–1993, he was also an NEC Faculty Fellow.

Prof. Bouman is a member of SPIE and IS&T professional societies. He has been both Chapter Chair and Vice Chair of the IEEE Central Indiana Signal Processing Chapter. Currently, he is an associate editor of the IEEE TRANSACTIONS ON IMAGE PROCESSING, and a member of the IEEE Image and Multidimensional Signal Processing Technical Committee.